Modelling Interactions Within and Between Peptide Amphiphile Supramolecular Filaments

Ivan R. Sasselli,[1,2] Zois Syrgiannis,[1,2] Nicholas A. Sather,[1,3] Liam C. Palmer,[1,2] Samuel I. Stupp.[1,2,3,4,5,*]

[1]Simpson Querrey Institute for BioNanotechnology, Northwestern University, 303 East Superior Street, 11th floor, Chicago, IL 60611, USA

[2]Department of Chemistry, Northwestern University, 2145 Sheridan Road, Evanston, IL 60208, USA.

[3]Department of Materials Science and Engineering, Northwestern University, 2220 Campus Drive, Evanston, IL 60208, USA.

[4]Department of Medicine, Northwestern University, 676 N St. Clair, Chicago, IL 60611, USA

[5]Department of Biomedical Engineering, Northwestern University, 2145 Sheridan Road, Evanston, IL 60208, USA.

supramolecular polymers, self-assembly, peptide amphiphiles, superstructure, nanofibers, molecular dynamics, coarse-grained simulations, supramolecular filaments, supramolecular biomaterials

ABSTRACT

Many peptides are able to self-assemble into 1-D nanostructures, such as cylindrical fibers or ribbons of variable widths, but the relationship between the morphology of 1-D objects and their molecular structure is not well understood. Here we use coarse-grained molecular dynamics (CG-MD) simulations to study the nanostructures formed by self-assembly of different peptide amphiphiles (PAs). The results show that ribbons are hierarchical superstructures formed by laterally assembled cylindrical fibers. Simulations starting from bilayer structures demonstrate the formation of filaments, whereas other simulations starting from filaments indicate varying degrees of interaction among them depending on chemical structure. These interactions are verified by observations using atomic force microscopy of the various systems. The interfilament interactions are predicted to be strongest in supramolecular assemblies that display hydrophilic groups on their surfaces, while those with hydrophobic ones are predicted to interact more weakly as confirmed by viscosity measurements. The simulations also indicate that peptide amphiphiles with hydrophobic termini bend to reduce their interfacial energy with water, which may explain why these systems do not collapse into superstructures of bundled filaments. The results suggest that future experiments will need to address mechanistic questions about the self-assembly of these systems into hierarchical structures, namely the preformation of interactive filaments *vs* equilibration of large assemblies into superstructures.

INTRODUCTION

Peptide matter is of broad interest across many scientific fields and functionally promising as a source of materials and nanostructures for advanced medicine, life-like robotic materials, and environmentally benign technologies.[1-10] This bio-inspired area of science takes advantage of the evolutionarily acquired ability of peptides to self-assemble into complex and highly functional architectures within living organisms.[7-9, 11-17] Supramolecular nanostructures formed by self-assembly of peptides or molecules containing peptide segments have emerged as an important family of structures that can be used as therapeutic constructs,[18-22] bioactive hydrogels,[23-30] and very recently as components in interesting membranes[31-33] and robotic materials.[3-4] The nanoscale morphology and mechanics of the supramolecular assemblies and bulk properties of the materials they form are controlled by amino acid sequences in their monomers and also self-assembly pathways.[34] A large variety of morphologies are known including spherical micelles,[35-36] cylindrical fibers,[17, 37-39] ribbons,[40-43] helices,[44-46] tubes,[8, 16, 47] and sheets,[14] among others.[15] The peptides used to form supramolecular structures can include biological signals for *in vivo* targeting,[19-21] protein binding, activation of receptors for signaling pathways,[44, 48-52] and drug delivery.[53-54] Additional efforts have been made recently to control interactions among supramolecular peptide nanostructures with the objective of building hierarchical architectures. This work has utilized DNA-base pairing and electrostatic interactions among peptides,[9, 55] calcium ions to build salt bridges,[23] as well as more specific host-guest interactions.[56-57]

Peptide amphiphiles (PAs), which are peptides commonly conjugated to alkyl segments or other non-polar moieties (such as aromatics or steroids) naturally exhibit a strong driving force to self-assemble in aqueous media driven by hydrophobic collapse.[17, 58-59] PAs developed in the Stupp laboratory form high aspect ratio nanostructures with a hydrophobic core formed by single aliphatic tails surrounded covalently bonded to peptides oriented perpendicular to the fiber axis, and commonly with a charged amino acid sequence that stabilizes interface of assemblies with water. These filamentous nanostructures can be functionalized with bioactive epitopes following the charged sequence to ensure surface display without significantly perturbing the filamentous nature, which is critical for their biological function and for their ability to form.[44, 48-49, 60-61] The design of the linker between the PA and the functional group has a major effect in both the bioactivity and structure.[60-61] In addition co-assembly between functionalized and non-bioactive PA molecules allows the control of functionalization density and minimization of any disruptive effects to architecture of supramolecular assemblies.[49, 62] Thus PA supramolecular polymers with filamentous morphology are particularly promising as bioactive scaffolds for tissue regeneration.[2, 63-64]

PAs are highly versatile and tunable building blocks, where both intermolecular cohesion and nanoscale morphology can be tuned. The intermolecular cohesion within the assemblies can be determined by β-sheet forming amino acid sequences,[65] while variations in pH or ionic strength can also have a major impact on morphology as a result of electrostatic interactions.[35, 39-40, 60] Other studies have demonstrated that the pathways used to form the nanostructure can affect morphology,[46] for example the length of filaments.[66] With regard to tunability of morphology, Cui *et al.* showed that varying the sequence of hydrophobic and charged amino acids on a tetrapeptide-based PA changes the nanostructure morphology from cylindrical fibers to ribbons.[41] Studies on crystalline packing within assemblies led to the hypothesis that changes in structure were the result of differences in side chain packing in cylindrical fibers *vs.* bilayer ribbons. However, the interactions responsible for these variations in supramolecular structure are not yet fully understood. Additionally, the ribbon thickness in these negatively charged PA nanostructures was shown to increase at lower pH values and attributed to the reduction of charge density leading ribbon-ribbon interactions.[40] Similarly, incorporation of hydrophobic epitopes for biological signaling to PAs tunes their supramolecular morphology from cylindrical fibers to ribbons and promotes bundling.[42, 44] Goldberger *et al.* showed that this effect could be reversed by increasing the number of negatively charged amino acids in peptide sequences which was found to affect bioactivity toward neurons.[42] Finally, the lateral assembly of fibers to form ribbons has been previously demonstrated for PAs with aromatic rather than aliphatic moieties.[13] More recent work on PAs has demonstrated the possibility of using DNA base pairing[9] and host-guest chemistry to form bundles.[56-57] At the same time, the control of interfilament interactions has also been linked recently to bulk mechanical properties of hydrogels by Sather *et al.*[67] In this work interfilamentous affinity could be tuned with pH and peptide sequence, similarly to the control of bundling and cylinder-to-ribbon transitions mentioned above. Therefore, understanding correlations between molecular structure and interactions among supramolecular filaments is of crucial importance to the functional design of PA nanostructures.

Despite great advances over the past two decades in the development of microscopy techniques, it has been challenging to obtain detailed molecular level information in supramolecular nanostructures. Access to such details would obviously facilitate the possibility of establishing the connection between molecular and supramolecular structure which is of great importance from a functional perspective. At least in some examples, molecular dynamics (MD) simulations have helped fill gaps in our understanding of supramolecular systems.[68] All-atom (AA) MD simulations have been used to obtain molecular level information such as secondary structure,[69-71] molecular orientation,[53, 72-76] water distribution[77-78] and thermodynamics[79-80] of PA nanostructures. However, these simulations are highly resource intensive, and

an initial starting structure is often required to accelerate convergence of the simulation. Furthermore, the initial structure limits the validity of the result as it can bias the simulation towards structures that are not experimentally relevant. Coarse-grained (CG) models sacrifice some of the atomistic resolution to reduce the computational cost of the simulations. Models such as MARTINI use a 4-1 mapping (*i.e.*, substituting every four heavy atoms with a single bead) to allow for timescales and system sizes that make it possible to simulate self-assembly without using an initial structure.[81-83] CG models have been shown to effectively reproduce polymorphism and water distribution of supramolecular peptide assemblies,[84-90] including PA systems.[91-93] The MARTINI force field has successfully been used to screen large libraries of peptides as a function of their self-assembly propensity leading to the discovery of new self-assembling tripeptides,[88-89] serving as starting point for the development of tripeptide based functional materials.[7, 94-96] Combinations of simulations with different levels of resolution (atomistic to coarse grained) have also been used to understand the role of water in fiber bundling.[77]

In this study, we aim to understand the internal supramolecular structure and its impact on interfilament interactions which can affect mechanical properties, superstructure formation, and bioactivity. For this purpose, we have utilized CG-MD simulations with the MARTINI force field to gain mechanistic insights on how filamentous assemblies interact to create larger scale structures. The PA molecules investigated here have an alkyl tail with 16 carbon atoms as the hydrophobic segment and four isomeric tetrapeptides that were previously shown experimentally to form different structures: C_{16}-VVEE-OH (VVEE, cylindrical fibers), C_{16}-VEVE-OH (VEVE, ribbons), C_{16}-EVEV-OH (EVEV, ribbons) and C_{16}-EEVV-OH (EEVV, fiber bundles) (Figure 1).[41]

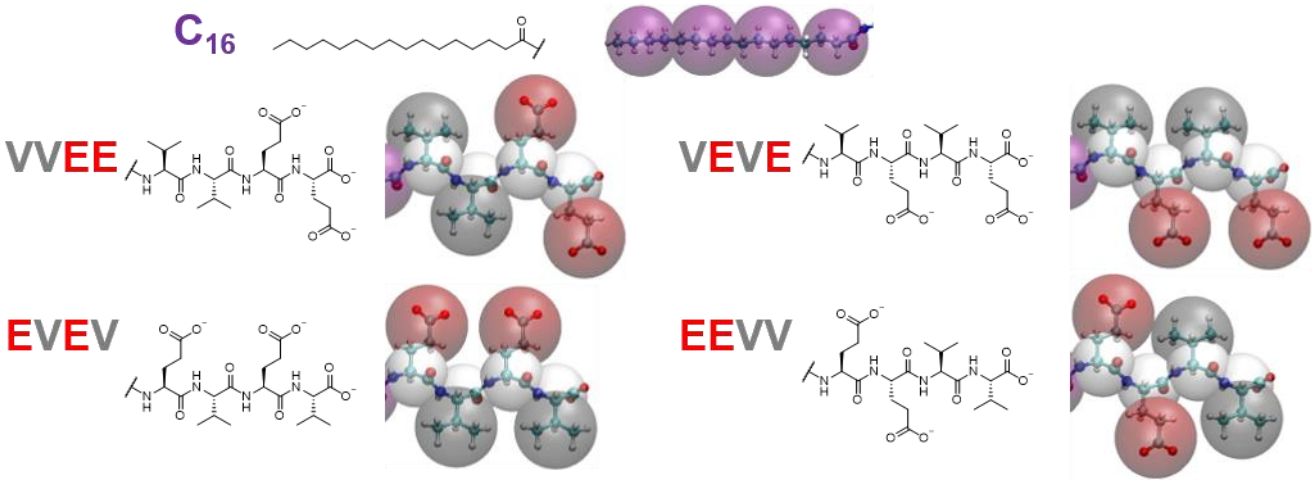

Figure 1. Peptide amphiphile structures used in this study. Coarse-grained (CG) representations of the structures are shown as transparent spheres over their respective atomistic ones. CG representations show the aliphatic tail in purple, amino acid residues with aliphatic side chains in grey (valine), amino acid residues with negatively charged side chains in red (glutamic acid), and the peptide backbone in white.

METHODS

Coarse Grained Molecular Dynamic Simulations

PA structures were built in Avogadro[97] and mapped to MARTINI 2.2[81-83] using a modified version of the *martinize.py* code to add the aliphatic tail.[83, 98] Coil secondary structures were used in all cases, which allows maximum backbone flexibility, avoiding parameters that force certain peptide conformations. All simulations were run in GROMACS 5.0.4.[99-100] The systems were investigated at variable charges to model differences in solution pH (0, -1, -1.5, -2 and -3). All visualizations were rendered using VMD (Visual Molecular Dynamics).[101] Further details can be found in the Supporting Information.

PA Sample Preparation

The four isomeric PA molecules with the following peptide sequences, EEVV, EVEV, VEVE and VVEE were synthetized using solid-phase peptide synthesis and purified in preparatory high-performance liquid chromatography (HPLC) following procedures described previously.[41] 500 µL samples at 10 mM were prepared in water with 1, 2 or 3 equivalents of NaOH (adding 1 µL/100µL of 1 M NaOH per equivalent). Each sample was bath sonicated until fully dissolved (~10 min) and then annealed (30 min at 80°C) followed by slowly cooling overnight.

Atomic Force Microscopy

Atomic force microscopy (AFM) samples were prepared by adding a drop of 5 µL of PA solution (1 mM, diluted from 10 mM) to the surface of freshly cleaved mica under ambient conditions (20°C and 50-60% humidity). The drop was washed three times with 150 mM aqueous NaCl and then incubated with 50 mM $CaCl_2$ (procedure was repeated twice). Samples were imaged with a Bruker Multimode -VIII AFM (Bruker) operating in "ScanAsyst mode in fluid" (Dimension FastScan, Bruker Corporation) with silicon nitride AFM cantilevers (Bruker, SNL10A) (Bruker Inc.).

Viscosity Curves

Viscosity curves of the four isomeric PAs using 600 µL 10 mM samples were collected using an Anton Paar MCR 302 rheometer with a cone–plate geometry (CP50-1 fixture). Careful consideration was taken to avoid bubbles and the samples were gently poured onto the bottom plate to minimize shear prior to measurement. Each sample was allowed to reach steady state within 1% allowance before measuring the next point.

RESULTS AND DISCUSSION

Initial studies on the PAs were carried out with self-assembly simulations starting from molecules randomly positioned in space (fully dissolved) (Figure 2a). These simulations allow us to study

nanostructure formation from randomly distributed molecules in solution without any bias in their initial configuration. For this purpose, 300 or 600 randomly distributed molecules were placed in the box with initial dimensions of 17.1 nm per side, corresponding to concentrations of 100 mM or 200 mM, respectively. These values are consistent with a tenfold increase in concentration that is frequently used to favor self-assembly over practical simulation timescales.[89-91, 102] The results of these simulations suggested a tendency of the molecules to form hierarchical superstructures. This is supported by having multiple C_{16} aggregates unlike systems prone to forming simple structures with a single continuous core of C_{16} tails. However, it was often not clear if this was due to a tendency to form larger disordered structures (*i.e.*, an "aggregate of aggregates") rather than a more organized superstructure of filaments. Therefore, different initial structures were used to model various steps of the proposed mechanisms (Figure S1). Simulations to equilibrate initially formed fibers were used as model systems to study the stability and structure of the filaments (Figure S1d). These fibers consist of 300 PA molecules in a 17.1 nm sided box (100 mM). Two replicas of each equilibrated fiber were included in a 27 nm long box to simulate the interaction between nanostructures (Figure S1f-e). Finally, in order to simulate initial aggregates in 2D, a bilayer was used as the initial structure (Figure S1c). These simulations begin with 968 PA molecules arranged in a bilayer (484 PA molecules/layer, 325 mM) with the aliphatic tails forming a 2D hydrophobic layer sandwiched between peptide layers, as in the model proposed by Cui *et al.* for VEVE and EVEV PAs.[41] It should be noted that although the ribbons are not strictly 2D, they can be considered as such on the scale of the simulations (17 nm sided boxes). After 10 μs of simulation (Figure 2b) all four systems at -1 charge/PA molecule remain stable in the 2D morphology, but we observed some differences in the orientation of the PA molecules relative to the initial bilayer. The results reveal the aliphatic region is oriented in laterally aggregated filaments for VEVE, EVEV and EEVV PAs (these filaments interact through peptide–peptide interactions). In this configuration the peptides are placed in antiparallel arrangements, distinct from the parallel peptide–peptide interactions among molecules of the same filament proposed by Cui *et al.* for VEVE and EVEV PAs.[41] This type of structure is closer to the one proposed for EEVV PA, although in that case the lateral aggregation of fibers happens in all directions rather than in only one plane. Therefore, the simulation is suggesting that the bundles and the ribbons are both superstructures. These three supramolecular structures (EEVV, EVEV and VEVE PAs) show differences in interdigitation of the peptides from interacting filaments. EEVV PA is the most interdigitated, making it the most efficiently packed. Due to this packing, the PAs are not able to completely fill the *xy*-plane, creating a gap (Figure 2b EEVV, blue area represents water in the gap). In the EVEV PA, peptide segments are less interdigitated and hence can better fill the surface (Figure 2b

EVEV). VEVE PA is the least interdigitated and the higher surface area makes the structure bend, situating the central fiber slightly out of the plane (Figure 2b VEVE). The differences in interdigitation are probably related to the changes in the dimensionality of these superstructures. In contrast to the ribbon-forming PAs, VVEE PA shows holes appearing in the bilayer (Figure 2b VVEE) and, hence, it is not able to stabilize the 2D disposition which is consistent with formation of cylindrical fibers.[41] The preferential arrangement of PA molecules in nanoscale filaments was also revealed in simulations starting from a random configuration (Figure 2a). Nevertheless, EEVV and EVEV PAs form more complex structures in which the aliphatic core is patchy rather than the continuum phase expected for ideal cylindrical nanofibers. This patchy nature occurs because the strong antiparallel peptide–peptide interactions prevent the formation of a continuous aliphatic core. When these peptide-peptide interactions occur among different filaments one would expect formation of superstructures. We also tried higher concentrations to check whether the superstructures would be more likely to occur but found instead that the limited size of the system and the tendency to connect through the periodic boundaries caused formation of branched structures. The initial bilayer structure was found to be critical in order to ensure the flat morphology characteristic of a ribbon section in results from the simulations.

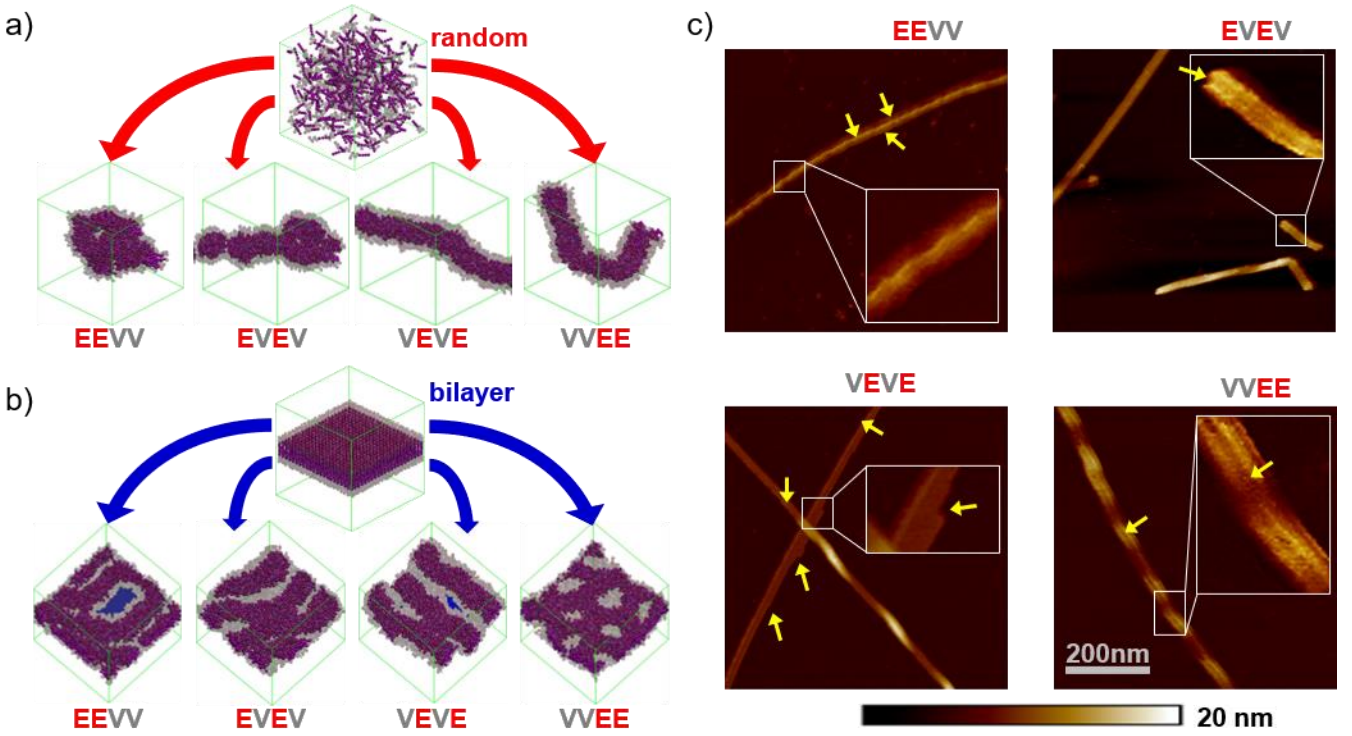

Figure 2. (a) Final structures obtained from simulations with PA molecules initially disposed randomly or in a bilayer configuration (b) (blue areas show structural gaps full of water, and structures are shown with the C_{16} hydrophobic segment in purple and the peptide part is made semi-transparent ; top boxes show the initial structures and the simulation box is shown in green and water and ions removed for clarity) (c) Experimental AFM images

of assemblies of the four isomers (yellow arrows indicate structural features that reveal the superstructure nature of the imaged objects and the insets show 100 nm wide zoomed images).

The superstructured nature of the ribbons may explain the narrow distribution of widths of the objects formed.[41] For example, we have previously reported on self-assembled nanoribbons with characteristic internal patterns that are consistent with the formation of superstructures.[44] The PAs in these examples commonly present hydrophobic side chains close to the surface of the fiber, favoring hydrophobic interactions among side chains of different filaments. The interfilamentous hydrophobic interactions driving the formation of superstructures is consistent with previous atomistic simulations on aromatic peptide amphiphiles.[13] Previous work on VEVE PA by Cui *et al.* at different pH values reported TEM images of ribbons with regular longitudinal patterns,[40] which are consistent with a hierarchical superstructure formed by laterally assembled filaments. In that work decreasing values of pH, and hence the number of charged glutamic acids, led the VEVE PA to form multilayered ribbon-shaped structures, consistent with the uncharged PA structures obtained in the bilayer simulations (Figure S6). EEVV PA simulated structure after 5 μs starting from randomly distributed molecules is the thickest as it is formed by the lateral interaction of up to 5 filaments (with aliphatic cores not connected between them). This is consistent with the wide structures observed experimentally for this PA, formed by filaments aggregated in multiple directions.[41]

Atomic force microscopy (AFM) was used to study the structures formed by these isomers. The excellent height resolution afforded by AFM clearly reveals the superstructure nature in assemblies of the EEVV PA (Figure 2c). However, the superstructure is also apparent to a lesser extent for VEVE and EVEV PAs, where we observed lines along the ribbons and some broken pieces of the ribbons (see yellow arrows in Figure 2c) that reveal the multifilament composition of the ribbons. The widths of the superstructures can be reduced by increasing the charge (Figure S27), consistent with the previously reported pH responsiveness of supramolecular assemblies of these molecules.[40] Therefore, the results suggest that these ribbons might be multifilament superstructures.

Given the importance of interfilament interactions in the formation of superstructures common in biological systems, the design of functional PA materials requires a deeper understanding of how they form in synthetic systems. Interactions among fibers is investigated here by placing two previously equilibrated fibers within interacting distance (surfaces within 1 nm) and re-equilibrating the system for 10 μs. Depending on the PA sequence and the charge state, some of the systems remain together through the whole simulation, suggesting strong interfilament interactions while others drift apart from each other when charge is increased, thus indicating coulombic repulsion (Figure 3a-c). Repulsion with increasing

charge causes a remarkable drop in interfilamentous affinity (Figure 3d). The four tetrapeptides investigated here reveal sufficient interfilamentous affinity to keep two fibers in close proximity throughout the simulation time used for up to -1 charge/PA (Figure 3a, Figure S11). However, at -1.5, EEVV PA and EVEV PA fibers start separating, while VEVE PA and VVEE PA remain within interacting distance up to -2 charge/PA (Figure 3b, c, f). The evolution of the interfiber distance with time for -2 charge/PA suggests how VEVE and VVEE PAs fibers interact over the last 5 μs of the simulation (Figure 3f). The average interfiber distance (Figure 3g) indicates that VVEE PA and VEVE PA fibers remain within interacting distance at the end of the simulation, while EEVV PA and EVEV PA structures separate above -1 charge/PA.

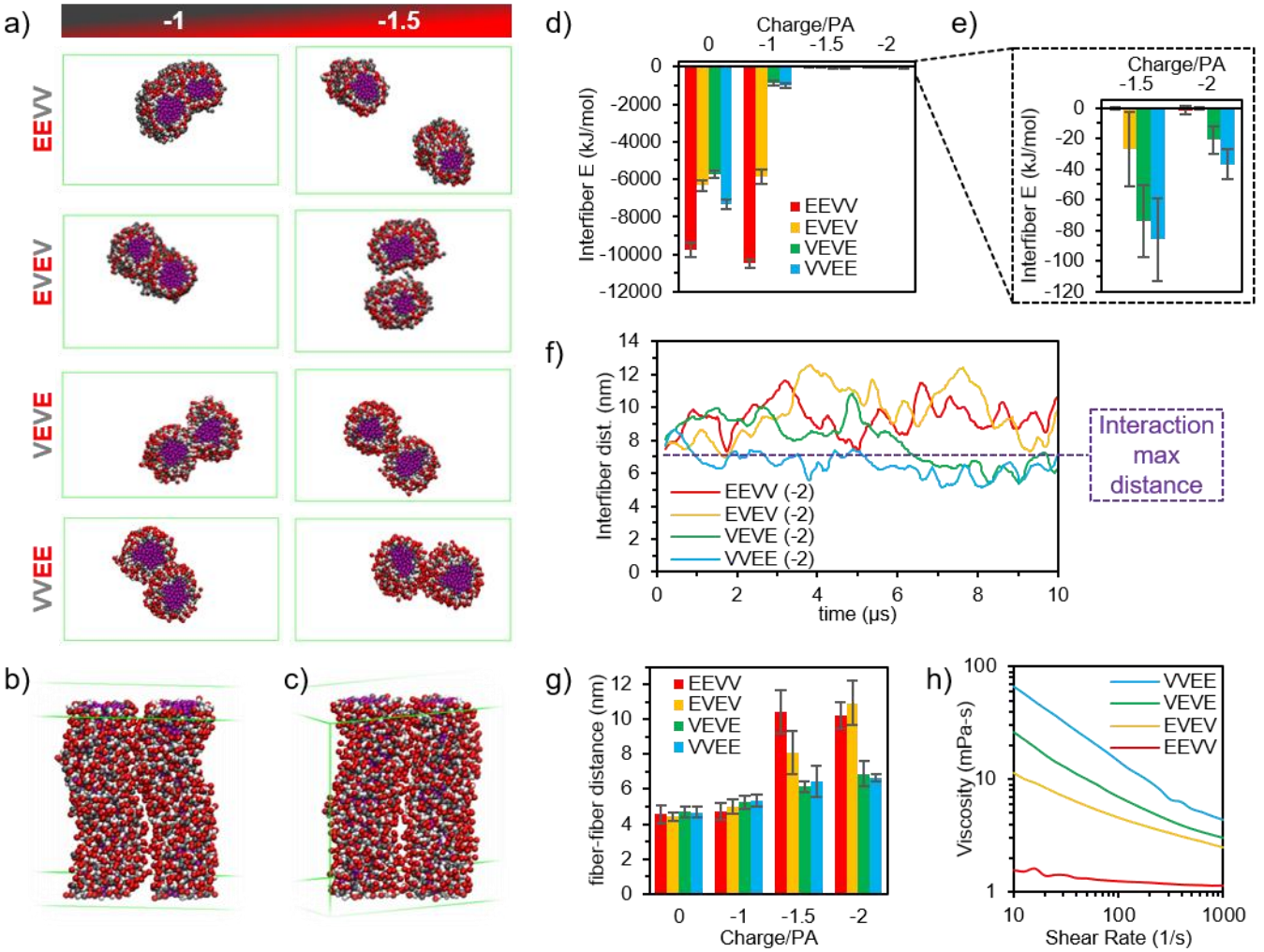

Figure 3. Final structures of the simulations with two fibers: (a) top view of the -1 and -1.5 charge/PA for the four different isomers and front view of the -2 charge/PA for VEVE (b) and VVEE (c); structures are shown with the aliphatic tail in purple, peptide backbone in white, hydrophobic side chains in grey, and hydrophilic side chains in red (the simulation box is shown in green and water and ions are omitted for clarity).; (d) Interfiber energies of the four isomers at different charge/PA and (e) expanded view the -1.5 and -2 charge/PA (e); (f) interfiber distance with time for the four isomers at -2 charge/PA, average value in the last 5 μs of the simulations(g), and experimentally measured viscosity curves (h).

The interfiber interaction energy shows that EEVV PA has the strongest interaction energy at zero charge and -1 (Figure 3d), which is consistent with the observed interdigitation (with a distance between aliphatic cores of 0.8 – 1.2 nm, which is less than twice the extended peptide part of the PA, ~1.6–2.0 nm) shown in Figure 2b. At 0 charge/PA molecule, the VVEE PA shows a stronger interaction than VEVE and EVEV PAs and at -1 VVEE PA remains stronger than VEVE PA. Although the interactions decrease at -1.5 and -2 charge/PA (Figure 3e), the interfiber distance analysis suggests that those small energies are still sufficient to keep the fibers together (Figure 3f). At these values of charge/PA molecule, the simulations show that the interfiber energy trend is: VVEE > VEVE > EVEV > EEVV. Hence, the PAs with the hydrophobic valine side chains closest to termini of the molecules and charged glutamic acid residues closer to the hydrophobic core would show weaker interfiber interactions than those with the highest charge density on the surface of nanostructures, which would presumably enhance interfiber charge repulsion. It is noteworthy that this preferential interfiber affinity with the greatest number of glutamic acid residues furthest from the core, arises when those side chains become charged (at charge -1 the terminal carboxylic group is charged but not the glutamic acid side chains, which only becomes charged at a net charge of -1.5/PA). This trend in interfilamentous affinity correlates with viscosity measured experimentally with 1 equivalent of NaOH (Figure 3h). At 2 equivalents all the viscosities decrease, as predicted by the simulations (Figure 3d-e) due to the disruptive effect of higher charges on interfiber interactions (Figure S28). Upon the addition of a second equivalent of base, VVEE viscosity drops below that of VEVE and EVEV PAs. This could be explained on the basis that VVEE molecules experience a stronger charge increment with the second equivalent due to the lower pK_a expected for the more external, and hence solvated, acid groups (*i.e.*, they are easier to deprotonate). Therefore, the affinity among previously equilibrated nanofibers correlates with the experimentally measured viscosity and not with superstructure formation, which, instead, follows the trend EEVV > EVEV > VEVE > VVEE. The fact that the simulations starting from bilayer structures reproduce the trends in superstructure formation but the interactions among filaments do not, suggests that the superstructures discussed are not formed upon the assembly of preexisting fibers through fiber-fiber interactions, but their formation is associated with the equilibration of large assemblies into interacting filaments as a result of electrostatic repulsion. For that reason, superstructures would form through a process similar to the one modelled by the molecules initially arranged in bilayers (as a model of the initial step of aggregation).

We sought to understand why nanostructures formed by PA molecules with hydrophobic residues near their surfaces do not show stronger interfilamentous affinity. This involved the in-depth analysis of the equilibrated fibers, which were the initial structures used to study the interactions between fibers. Using

the same initial fiber structure, the different tetrapeptides are equilibrated through 5 μs at different charge/PA. All the fibers were stable (Figure 4a) up to -2 charge/PA but converted into micelles at -3 charge/PA (Figure S8). Therefore, the influence of the charges on glutamic acid side chains could only be assessed in the glutamic acid residues placed furthest from the aliphatic tail, closest to the C-termini. The fibers elongate as intermolecular distance increases with charge due to the repulsion among neighboring PAs (Figure 4b). The strength of the repulsion depends on the position of the most external glutamic acid residues, where the second negative charged is added. EEVV and EVEV PAs show the biggest elongation upon addition of the second charge, while VEVE and VVEE PAs exhibit minimal elongation relative to the -1 charge state. This affects the charge density of the fibers (Figure 4c), where the PAs with the most external E amino acids show higher charge density. Even at charge 0 and -1, EEVV and EVEV PAs form longer fibers than VEVE and VVEE PAs even though they both have a -1 charge/PA at the C-terminal carboxylic acid. Therefore, the structural changes promoting these differences must be induced by the different distribution of hydrophilic and hydrophobic side chains.

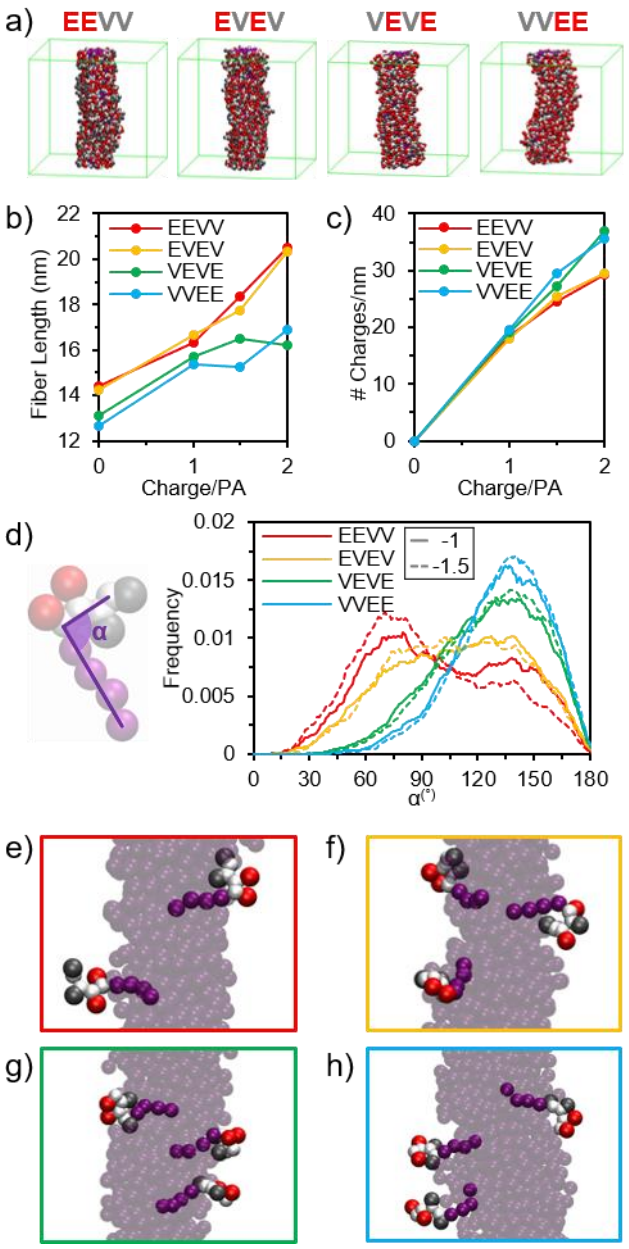

Figure 4. (a) Final structures of the fiber equilibration simulations for the four isomers; (b) Fiber length and (c) charge density for the four isomers as a function of the charge/PA molecule. (d) PA extension analysis (using the occurrence frequency among all the PA molecules in the fiber of the angle α, shown in the scheme) for the four isomers at -1 and -1.5 charge/PA. Illustration showing examples of PA molecules conformations within the fibers shown in (a) for EEVV (e), EVEV (f), VEVE (g) and VVEE (h) (in a and e-h structures are shown with the C_{16} in purple, peptide backbone in white, hydrophobic side chains in grey, and hydrophilic side chains in red; simulation box is shown in green, water and ions are omitted for clarity; in e-h the aliphatic core is transparent and most PAs are removed to show the orientation of certain PAs within the nanofibers).

Previous all-atom MD simulations for PA assemblies used initial structures in which PA molecules have radial orientation orthogonal to the *z*-axis (fiber axis).[74, 76, 80] However, the PAs studied here show deviations from this ideal behavior. The PA extension is analyzed using the backbone (BB) bead of the first (BB_1) and last (BB_4) amino acid and the C_{16} bead ($SC3_{C16}$) most distant from the peptide (Figure 4d,

scheme). The greater the angle α, the more extended the PAs are. VVEE shows the maximum population of PA molecules with an angle of around 135° (Figure 4d), corresponding to an extended structure whereas VEVE PA which shows a small decrease in the 135° population in favor of bent PA molecules with α values of 90°. EVEV and EEVV PAs show a high population of bent PA molecules with the EVEV PA having equal populations of molecules bent 75° and 135°, whereas EEVV PA has its main population bent at 75° (Figure 4d). While this bending effect has not been previously reported for PAs, Matson *et al.* used the bending of a hydrophobic moiety to explain changes in PA packing.[103] The bending of their moiety was more pronounced as it was closer to the hydrophilic part of the PA. Similarly, the bending of our isomers appears to be most dramatic when the most external glutamic acid side chain is closer to the aliphatic tail, locating the negatively charged carboxylate within the nanostructure, close to the aliphatic core. Hence, EEVV PA shows the greatest increment in bent PA molecules at -1.5 relative to -1 charge/PA molecule. Overall, molecular bending follows the order, EEVV > EVEV > VEVE > VVEE suggesting that bending occurs when molecules have hydrophobic side chains further from the aliphatic tail (Figure 4d). This bending difference explains the fiber length variations among PAs (Figure 4b) because bent molecules occupy more fiber surface, causing an elongation of the fiber and a corresponding decrease in charge density (Figure 4c). The simulations suggest that bending occurs to allow the hydrophobic side chains (Figure 4e-g) to lie closer to the hydrophobic core of the fiber and the carboxylic acid side chains to become more exposed to the solvent, stabilizing the hydrophobic/hydrophilic interface PA nanostructures. The VVEE PA does not bend (Figure 4d, h) as it has a frequently used molecular design which creates maximal amphiphilicity using a gradient of hydrophobicity from the most hydrophobic (C_{16}) to the most hydrophilic (charged region) with intermediate hydrophobicity amino acids between them (commonly valines and alanines). The results suggest that this type of PA design favors the ideal radial orientation of extended PA molecules.

Based on results discussed above we conclude that although PA molecules with external V residues are expected to have greater interfilament affinity due to the higher number of exposed hydrophobic side chains in the ideal radial configuration, the bending to stabilize the interface with water avoids the high hydrophobic exposure. This explains the differences in interfiber affinity observed in pre-equilibrated fibers (Figure 3) and superstructures formed from large aggregates (bilayer initial structure, figure 2b). Consequently, the results suggest that superstructures are not formed by pre-existing fibers that assemble but from the equilibration of large assemblies into strongly interacting filaments (as observed in bilayer simulations). We conclude that the interactions among pre-formed fibers are responsible for the

rheological properties, as shown by the agreement between experimental viscosity measurements and the simulations on interfilamentous affinity (Figure 3).

CONCLUSIONS

In this work we have employed CG-MD simulations to investigate superstructures of nanoscale ribbons formed by the self-assembly of three peptide amphiphiles, C_{16}-VEVE-OH, C_{16}-EVEV-OH and C_{16}-EEVV-OH. Our results have also shed some light on the formation mechanism of these superstructures, suggesting that it may not be driven by interfilamentous affinity of pre-formed fibers, but rather on the equilibration of large supramolecular assemblies. The presence of hydrophobic residues, valines in this case, close to the C-terminus of molecules exposed to water enhances peptide–peptide interactions among filaments. The greater interdigitation of molecules in the C_{16}-EEVV-OH PA suggests a stronger affinity promoting interfilamentous interactions in all directions and thus giving rise to bundles, instead of just planar ribbons. We have also shown that the interactions among pre-formed filaments follows the opposite trend, with C_{16}-VVEE-OH establishing the strongest interactions, followed by C_{16}-VEVE-OH, C_{16}-EVEV-OH and C_{16}-EEVV-OH. Hence, these interactions are predicted to be strongest in supramolecular assemblies of PA molecules with hydrophilic residues closest to their more exposed C-terminus, while those with a higher exposure of hydrophobic residues display weaker interactions. This correlates with the experimentally measured viscosity of the materials. The simulations suggest that the PA molecules with hydrophobic termini bend to bury these groups within the filament, reducing the interfacial energy with water. The lower exposure of hydrophobic residues may explain the lower interactions among these filaments and why these systems do not collapse into superstructures of bundled filaments. This finding supports fully extended molecules occur with the usual PA design with a decreasing gradient of hydrophobicity from the tail to the charged C-terminus. Overall, our simulations have led us to some insights on the nature of interfilamentous interactions and superstructures formed by PA assemblies.

ASSOCIATED CONTENT

Supporting Information. Further simulations details and results. This material is available free of charge via the Internet at http://pubs.acs.org.

AUTHOR INFORMATION

Corresponding Author

* s-stupp@northwestern.edu

Notes

The authors declare no competing financial interest.

ACKNOWLEDGMENTS

This work was primarily supported by the US Department of Energy, Office of Science, Basic Energy Sciences, under awards numbers DE-SC0020884 (for coarse-grained simulations). Additional support for the AFM characterization was provided by the Center for Bio-Inspired Energy Science (CBES), an Energy Frontier Research Center (EFRC) funded by the US Department of Energy, Office of Science, Basic Energy Sciences under award number DE-SC0000989. This research was supported in part by the computational resources and staff contributions provided by the Quest High Performance Computing Facility at Northwestern University which is jointly supported by the Office of the Provost, the Office for Research, and Northwestern University Information Technology. Peptide synthesis and purification were performed in the Peptide Synthesis Core Facility of the Simpson Querrey Institute at Northwestern University. IRS wants to dedicate this work to Paula Gonzalez Garcia, without her support this would not have been possible.

ABBREVIATIONS

PA, peptide amphiphile; CG-MD, Coarse-grained molecular dynamics; VVEE, C_{16}-VVEE-OH; VEVE, C_{16}-VEVE-OH; EVEV, C_{16}-EVEV-OH; EEVV, C_{16}-EEVV-OH; AFM, atomic force microscopy; C_{16}, palmitoyl; V, valine; A, alanine; E, glutamic acid.

REFERENCES

1. Pappas, C. G.; Shafi, R.; Sasselli, I. R.; Siccardi, H.; Wang, T.; Narang, V.; Abzalimov, R.; Wijerathne, N.; Ulijn, R. V. Dynamic Peptide Libraries for Discovery of Supramolecular Nanomaterials. *Nat. Nanotechnol.,* **2016,** *11*, 960-967.
2. Cui, H.; Webber, M. J.; Stupp, S. I. Self-assembly of peptide amphiphiles: From molecules to nanostructures to biomaterials. *J. Pept. Sci.,* **2010,** *94*, 1-18.
3. Li, C.; Iscen, A.; Sai, H.; Sato, K.; Sather, N. A.; Chin, S. M.; Álvarez, Z.; Palmer, L. C.; Schatz, G. C.; Stupp, S. I. Supramolecular–covalent hybrid polymers for light-activated mechanical actuation. *Nat. Mater.,* **2020,** *19*, 900-909.
4. Chin, S. M.; Synatschke, C. V.; Liu, S.; Nap, R. J.; Sather, N. A.; Wang, Q.; Álvarez, Z.; Edelbrock, A. N.; Fyrner, T.; Palmer, L. C.; Szleifer, I.; Olvera de la Cruz, M.; Stupp, S. I. Covalent-supramolecular hybrid polymers as muscle-inspired anisotropic actuators. *Nat. Commun.,* **2018,** *9*, 2395.
5. Lee, M. J.; Mantell, J.; Brown, I. R.; Fletcher, J. M.; Verkade, P.; Pickersgill, R. W.; Woolfson, D. N.; Frank, S.; Warren, M. J. De novo targeting to the cytoplasmic and luminal side of bacterial microcompartments. *Nat. Commun.,* **2018,** *9*, 1-11.
6. Adler-Abramovich, L.; Gazit, E. The Physical Properties of Supramolecular Peptide Assemblies: From Building Block Association to Technological Applications. *Chem. Soc. Rev.,* **2014,** *43*, 6881-6893.
7. Lampel, A.; McPhee, S. A.; Park, H.-A.; Scott, G. G.; Humagain, S.; Hekstra, D. R.; Yoo, B.; Frederix, P. W.; Abzalimov, R. R.; Greenbaum, S. G.; Tuttle, T.; Hu, C.; Bettinger, C. J.; Ulijn, R. V. Polymeric peptide pigments with sequence-encoded properties. *Science,* **2017,** *356*, 1064-1068.

8. Reches, M.; Gazit, E. Casting Metal Nanowires within Discrete Self-assembled Peptide Nanotubes. *Science,* **2003,** *300*, 625-627.
9. Freeman, R.; Han, M.; Álvarez, Z.; Lewis, J. A.; Wester, J. R.; Stephanopoulos, N.; McClendon, M. T.; Lynsky, C.; Godbe, J. M.; Sangji, H.; Luijten, E.; Stupp, S. I. Reversible self-assembly of superstructured networks. *Science,* **2018,** *362*, 808-813.
10. Young, D. D.; Schultz, P. G. Playing with the molecules of life. *ACS Chem. Biol.,* **2018,** *13*, 854-870.
11. Whitesides, G. M.; Grzybowski, B. Self-assembly at all scales. *Science,* **2002,** *295*, 2418-2421.
12. Zhang, S. Fabrication of Novel Biomaterials Through Molecular Self-assembly. *Nat. Biotechnol.,* **2003,** *21*, 1171-1178.
13. Sasselli, I. R.; Pappas, C. G.; Matthews, E.; Wang, T.; Hunt, N.; Ulijn, R.; Tuttle, T. Using experimental and computational energy equilibration to understand hierarchical self-assembly of Fmoc-dipeptide amphiphiles. *Soft Matter,* **2016,** *12*, 8307-8315.
14. Hughes, M.; Frederix, P. W. J. M.; Raeburn, J.; Birchall, L. S.; Sadownik, J.; Coomer, F. C.; Lin, I. H.; Cussen, E. J.; Hunt, N. T.; Tuttle, T.; Webb, S. J.; Adams, D. J.; Ulijn, R. V. Sequence/Structure Relationships in Aromatic Dipeptide Hydrogels Formed Under Thermodynamic Control by Enzyme-assisted Self-assembly. *Soft Matter,* **2012,** *8*, 5595-5602.
15. Erdogan, H.; Babur, E.; Yilmaz, M.; Candas, E.; Gordesel, M.; Dede, Y.; Oren, E. E.; Demirel, G. B.; Ozturk, M. K.; Yavuz, M. S. Morphological versatility in the self-assembly of Val-Ala and Ala-Val dipeptides. *Langmuir,* **2015,** *31*, 7337-7345.
16. Burgess, N. C.; Sharp, T. H.; Thomas, F.; Wood, C. W.; Thomson, A. R.; Zaccai, N. R.; Brady, R. L.; Serpell, L. C.; Woolfson, D. N. Modular design of self-assembling peptide-based nanotubes. *J. Am. Chem. Soc.,* **2015,** *137*, 10554-10562.
17. Hartgerink, J. D.; Benlash, E.; Stupp, S. L. Self-Assembly and Mineralization of Peptide-Amphiphile Nanofibers. *Science,* **2001,** *294*, 1684-1688.
18. Moyer, T. J.; Chen, F.; Toft, D. J.; Ruff, Y.; Cryns, V. L.; Stupp, S. I. Self-assembled peptide nanostructures targeting death receptor 5 and encapsulating paclitaxel as a multifunctional cancer therapy. *ACS Biomater. Sci. Eng.,* **2019,** *5*, 6046-6053.
19. Kalafatovic, D.; Nobis, M.; Son, J.; Anderson, K. I.; Ulijn, R. V. MMP-9 triggered self-assembly of doxorubicin nanofiber depots halts tumor growth. *Biomaterials,* **2016,** *98*, 192-202.
20. Morgan, C. E.; Dombrowski, A. W.; Rubert Pérez, C. M.; Bahnson, E. S.; Tsihlis, N. D.; Jiang, W.; Jiang, Q.; Vercammen, J. M.; Prakash, V. S.; Pritts, T. A.; Stupp, S. I.; Kibbe, M. R. Tissue-factor targeted peptide amphiphile nanofibers as an injectable therapy to control hemorrhage. *ACS Nano,* **2015,** *10*, 899-909.
21. Bahnson, E. S.; Kassam, H. A.; Moyer, T. J.; Jiang, W.; Morgan, C. E.; Vercammen, J. M.; Jiang, Q.; Flynn, M. E.; Stupp, S. I.; Kibbe, M. R. Targeted nitric oxide delivery by supramolecular nanofibers for the prevention of restenosis after arterial injury. *Antioxid. Redox Signaling,* **2016,** *24*, 401-418.
22. Okesola, B. O.; Ni, S.; Derkus, B.; Galeano, C. C.; Hasan, A.; Wu, Y.; Ramis, J.; Buttery, L.; Dawson, J. I.; D'Este, M. Growth-Factor Free Multicomponent Nanocomposite Hydrogels That Stimulate Bone Formation. *Adv. Funct. Mater.,* **2020,** *30*, 1906205.
23. Alakpa, E. V.; Jayawarna, V.; Lampel, A.; Burgess, K. V.; West, C. C.; Bakker, S. C.; Roy, S.; Javid, N.; Fleming, S.; Lamprou, D. A.; Yang, J.; Miller, A.; Urquhart, A. J.; Frederix, P. W. J. M.; Hunt, N. T.; Peault, B.; Ulijn, R. V.; Dalby, M. J. Tunable supramolecular hydrogels for selection of lineage-guiding metabolites in stem cell cultures. *Chem,* **2016,** *1*, 298-319.
24. Silva, G. A.; Czeisler, C.; Niece, K. L.; Beniash, E.; Harrington, D. A.; Kessler, J. A.; Stupp, S. I. Selective differentiation of neural progenitor cells by high-epitope density nanofibers. *Science,* **2004,** *303*, 1352-1355.
25. Lee, S. S.; Fyrner, T.; Chen, F.; Álvarez, Z.; Sleep, E.; Chun, D. S.; Weiner, J. A.; Cook, R. W.; Freshman, R. D.; Schallmo, M. S.; Katchko, K. M.; Schneider, A. D.; Smith, J. T.; Yun, C.; Singh, G.; Hashmi, S. Z.; McClendon, M. T.; Yu, Z.; Stock, S. R.; Hsu, W. K.; Hsu, E. L.; Stupp, S. I. Sulfated glycopeptide nanostructures for multipotent protein activation. *Nat. Nanotechnol.,* **2017,** *12*, 821-829.
26. Huang, Z.; Sargeant, T. D.; Hulvat, J. F.; Mata, A.; Bringas Jr, P.; Koh, C. Y.; Stupp, S. I.; Snead, M. L. Bioactive nanofibers instruct cells to proliferate and differentiate during enamel regeneration. *J. Bone Miner. Res.,* **2008,** *23*, 1995-2006.
27. Sleep, E.; Cosgrove, B. D.; McClendon, M. T.; Preslar, A. T.; Chen, C. H.; Sangji, M. H.; Pérez, C. M. R.; Haynes, R. D.; Meade, T. J.; Blau, H. M. Injectable biomimetic liquid crystalline scaffolds enhance muscle stem cell transplantation. *Proc. Natl. Acad. Sci.,* **2017,** *114*, E7919-E7928.

28. Ustun Yaylaci, S.; Sardan Ekiz, M.; Arslan, E.; Can, N.; Kilic, E.; Ozkan, H.; Orujalipoor, I.; Ide, S.; Tekinay, A. B.; Guler, M. O. Supramolecular GAG-like self-assembled glycopeptide nanofibers induce chondrogenesis and cartilage regeneration. *Biomacromolecules,* **2016,** *17*, 679-689.
29. de la Peña, D. O.; Trabulo, S.; Collin, E.; Loessner, D.; Mata, Á.; Heeschen, C. Self-assembling biomimetic hydrogels as a novel 3D in vitro platform for pancreatic cancer research. *Pancreatology,* **2020,** *20*, e7.
30. Tysseling-Mattiace, V. M.; Sahni, V.; Niece, K. L.; Birch, D.; Czeisler, C.; Fehlings, M. G.; Stupp, S. I.; Kessler, J. A. Self-assembling nanofibers inhibit glial scar formation and promote axon elongation after spinal cord injury. *J. Neurosci.,* **2008,** *28*, 3814-3823.
31. Capito, R. M.; Azevedo, H. S.; Velichko, Y. S.; Mata, A.; Stupp, S. I. Self-assembly of large and small molecules into hierarchically ordered sacs and membranes. *Science,* **2008,** *319*, 1812-1816.
32. Borges, J.; Sousa, M. P.; Cinar, G.; Caridade, S. G.; Guler, M. O.; Mano, J. F. Nanoengineering Hybrid Supramolecular Multilayered Biomaterials Using Polysaccharides and Self-Assembling Peptide Amphiphiles. *Adv. Funct. Mater.,* **2017,** *27*, 1605122.
33. Ribeiro, S.; Radvar, E.; Shi, Y.; Borges, J.; Pirraco, R. P.; Leonor, I. B.; Mano, J. F.; Reis, R. L.; Mata, Á.; Azevedo, H. S. Nanostructured interfacial self-assembled peptide–polymer membranes for enhanced mineralization and cell adhesion. *Nanoscale,* **2017,** *9*, 13670-13682.
34. Korevaar, P. A.; Newcomb, C. J.; Meijer, E.; Stupp, S. I. Pathway Selection in Peptide Amphiphile Assembly. *J. Am. Chem. Soc.,* **2014,** *136*, 8540-8543.
35. Gao, C.; Li, H.; Li, Y.; Kewalramani, S.; Palmer, L. C.; Dravid, V. P.; Stupp, S. I.; Olvera de la Cruz, M.; Bedzyk, M. J. Electrostatic control of polymorphism in charged amphiphile assemblies. *J. Phys. Chem. B,* **2017,** *121*, 1623-1628.
36. Hutchinson, J. A.; Hamley, I. W.; Torras, J.; Alemán, C.; Seitsonen, J.; Ruokolainen, J. Self-Assembly of Lipopeptides Containing Short Peptide Fragments Derived from the Gastrointestinal Hormone PYY3–36: From Micelles to Amyloid Fibrils. *J. Phys. Chem. B,* **2019,** *123*, 614-621.
37. Han, S.; Cao, S.; Wang, Y.; Wang, J.; Xia, D.; Xu, H.; Zhao, X.; Lu, J. R. Self-Assembly of Short Peptide Amphiphiles: The Cooperative Effect of Hydrophobic Interaction and Hydrogen Bonding. *Chem.-Eur. J.,* **2011,** *17*, 13095-13102.
38. Yang, Z.; Gu, H.; Fu, D.; Gao, P.; Lam, J. K.; Xu, B. Enzymatic Formation of Supramolecular Hydrogels. *Adv. Mater,* **2004,** *16*, 1440–1444.
39. Ghosh, A.; Dobson, E. T.; Buettner, C. J.; Nicholl, M. J.; Goldberger, J. E. Programming pH-triggered self-assembly transitions via isomerization of peptide sequence. *Langmuir,* **2014,** *30*, 15383-15387.
40. Cui, H.; Muraoka, T.; Cheetham, A. G.; Stupp, S. I. Self-Assembly of Giant Peptide Nanobelts. *Nano Lett.,* **2009,** *9*, 945-951.
41. Cui, H.; Cheetham, A. G.; Pashuck, E. T.; Stupp, S. I. Amino acid sequence in constitutionally isomeric tetrapeptide amphiphiles dictates architecture of one-dimensional nanostructures. *J. Am. Chem. Soc.,* **2014,** *136*, 12461-12468.
42. Goldberger, J. E.; Berns, E. J.; Bitton, R.; Newcomb, C. J.; Stupp, S. I. Electrostatic control of bioactivity. *Angew. Chem.,* **2011,** *50*, 6292-6295.
43. Moyer, T. J.; Cui, H.; Stupp, S. I. Tuning nanostructure dimensions with supramolecular twisting. *J. Phys. Chem. B,* **2012,** *117*, 4604-4610.
44. Rubert Pérez, C. M.; Álvarez, Z.; Chen, F.; Aytun, T.; Stupp, S. I. Mimicking the Bioactivity of Fibroblast Growth Factor-2 Using Supramolecular Nanoribbons. *ACS Biomater. Sci. Eng.,* **2017,** *3*, 2166-2175.
45. Merg, A. D.; Boatz, J. C.; Mandal, A.; Zhao, G.; Mokashi-Punekar, S.; Liu, C.; Wang, X.; Zhang, P.; van der Wel, P. C.; Rosi, N. L. Peptide-directed assembly of single-helical gold nanoparticle superstructures exhibiting intense chiroptical activity. *J. Am. Chem. Soc.,* **2016,** *138*, 13655-13663.
46. Pashuck, E. T.; Stupp, S. I. Direct Observation of Morphological Tranformation from Twisted Ribbons into Helical Ribbons. *J. Am. Chem. Soc.,* **2010,** *132*, 8819-8821.
47. Li, S.; Mehta, A. K.; Sidorov, A. N.; Orlando, T. M.; Jiang, Z.; Anthony, N. R.; Lynn, D. G. Design of asymmetric peptide bilayer membranes. *J. Am. Chem. Soc.,* **2016,** *138*, 3579-3586.
48. Webber, M. J.; Tongers, J.; Newcomb, C. J.; Marquardt, K.-T.; Bauersachs, J.; Losordo, D. W.; Stupp, S. I. Supramolecular nanostructures that mimic VEGF as a strategy for ischemic tissue repair. *Proc. Natl. Acad. Sci.,* **2011,** *108*, 13438-13443.
49. Edelbrock, A. N.; Àlvarez, Z.; Simkin, D.; Fyrner, T.; Chin, S. M.; Sato, K.; Kiskinis, E.; Stupp, S. I. Supramolecular Nanostructure Activates TrkB Receptor Signaling of Neuronal Cells by Mimicking Brain-Derived Neurotrophic Factor. *Nano Lett.,* **2018,** *18*, 6237-6247.

50. Zhou, M.; Smith, A. M.; Das, A. K.; Hodson, N. W.; Collins, R. F.; Ulijn, R. V.; Gough, J. E. Self-assembled peptide-based hydrogels as scaffolds for anchorage-dependent cells. *Biomaterials,* **2009,** *30*, 2523-2530.
51. Xu, F.; Liu, J.; Tian, J.; Gao, L.; Cheng, X.; Pan, Y.; Sun, Z.; Li, X. Supramolecular self-assemblies with nanoscale RGD clusters promote cell growth and intracellular drug delivery. *ACS Appl. Mater. Interfaces,* **2016,** *8*, 29906-29914.
52. Rodriguez, A.; Wang, T.-Y.; Bruggeman, K.; Horgan, C.; Li, R.; Williams, R. J.; Parish, C. L.; Nisbet, D. In vivo assessment of grafted cortical neural progenitor cells and host response to functionalized self-assembling peptide hydrogels and the implications for tissue repair. *J. Mater. Chem. B,* **2014,** *2*, 7771-7778.
53. Mazza, M.; Notman, R.; Anwar, J.; Rodger, A.; Hicks, M.; Parkinson, G.; McCarthy, D.; Daviter, T.; Moger, J.; Garrett, N. Nanofiber-based delivery of therapeutic peptides to the brain. *ACS Nano,* **2013,** *7*, 1016-1026.
54. Tang, J. D.; Mura, C.; Lampe, K. J. A stimuli-responsive, pentapeptide, nanofiber hydrogel for tissue engineering. *J. Am. Chem. Soc.,* **2019**.
55. Wester, J. R.; Lewis, J. A.; Freeman, R.; Sai, H.; Palmer, L. C.; Henrich, S. E.; Stupp, S. I. Supramolecular exchange among assemblies of opposite charge leads to hierarchical structures. *J. Am. Chem. Soc.,* **2020,** *142*, 12216-12225.
56. Redondo-Gómez, C.; Abdouni, Y.; Becer, C. R.; Mata, A. Self-assembling hydrogels based on a complementary host-guest peptide amphiphile pair. *Biomacromolecules,* **2019**.
57. Edelbrock, A. N.; Clemons, T. D.; Chin, S. M.; Roan, J. J.; Bruckner, E. P.; Álvarez, Z.; Edelbrock, J. F.; Wek, K. S.; Stupp, S. I. Superstructured Biomaterials Formed by Exchange Dynamics and Host–Guest Interactions in Supramolecular Polymers. *Advanced Science,* **2021,** *8*, 2004042.
58. Hartgerink, J. D.; Beniash, E.; Stupp, S. I. Peptide-amphiphile nanofibers: a versatile scaffold for the preparation of self-assembling materials. *Proc. Natl. Acad. Sci.,* **2002,** *99*, 5133-5138.
59. Marullo, R.; Kastantin, M.; Drews, L. B.; Tirrell, M. Peptide contour length determines equilibrium secondary structure in protein-analogous micelles. *Biopolymers,* **2013,** *99*, 573-581.
60. Newcomb, C. J.; Sur, S.; Ortony, J. H.; Lee, O.-S.; Matson, J. B.; Boekhoven, J.; Yu, J. M.; Schatz, G. C.; Stupp, S. I. Cell death versus cell survival instructed by supramolecular cohesion of nanostructures. *Nat. Commun.,* **2014,** *5*, 1-10.
61. Sur, S.; Tantakitti, F.; Matson, J. B.; Stupp, S. I. Epitope topography controls bioactivity in supramolecular nanofibers. *Biomater. Sci.,* **2015,** *3*, 520-532.
62. Lee, S. S.; Hsu, E. L.; Mendoza, M.; Ghodasra, J.; Nickoli, M. S.; Ashtekar, A.; Polavarapu, M.; Babu, J.; Riaz, R. M.; Nicolas, J. D.; Nelson, D.; Hashmi, S. Z.; Kaltz, S. R.; Earhart, J. S.; Merk, B. R.; McKee, J. S.; Bairstow, S. F.; Shah, R. N.; Hsu, W. K.; Stupp, S. I. Gel scaffolds of BMP-2-binding peptide amphiphile nanofibers for spinal arthrodesis. *Adv. Health. Mat.,* **2015,** *4*, 131-141.
63. Berns, E. J.; Álvarez, Z.; Goldberger, J. E.; Boekhoven, J.; Kessler, J. A.; Kuhn, H. G.; Stupp, S. I. A tenascin-C mimetic peptide amphiphile nanofiber gel promotes neurite outgrowth and cell migration of neurosphere-derived cells. *Acta Biomater.,* **2016,** *37*, 50-58.
64. Aida, T.; Meijer, E.; Stupp, S. Functional Supramolecular Polymers. *Science,* **2012,** *335*, 813-817.
65. Pashuck, E. T.; Cui, H.; Stupp, S. I. Tuning supramolecular rigidity of peptide fibers through molecular structure. *J. Am. Chem. Soc.,* **2010,** *132*, 6041-6046.
66. Tantakitti, F.; Boekhoven, J.; Wang, X.; Kazantsev, R. V.; Yu, T.; Li, J.; Zhuang, E.; Zandi, R.; Ortony, J. H.; Newcomb, C. J.; Palmer, L. C.; Shekhawat, G. S.; Olvera de la Cruz, M.; Schatz, G. C.; Stupp, S. I. Energy landscapes and functions of supramolecular systems. *Nat. Mater.,* **2016**.
67. Sather, N. A.; Sai, H.; Sasselli, I. R.; Sato, K.; Ji, W.; Synatschke, C. V.; Zambrotta, R. T.; Edelbrock, J. F.; Kohlmeyer, R. R.; Hardin, J. O. 3D Printing of Supramolecular Polymer Hydrogels with Hierarchical Structure. *Small,* **2021,** *17*, 2005743.
68. Frederix, P. W.; Patmanidis, I.; Marrink, S. J. Molecular simulations of self-assembling bio-inspired supramolecular systems and their connection to experiments. *Chem. Soc. Rev.,* **2018,** *47*, 3470-3489.
69. Rad-Malekshahi, M.; Visscher, K. M.; Rodrigues, J. P.; De Vries, R.; Hennink, W. E.; Baldus, M.; Bonvin, A. M.; Mastrobattista, E.; Weingarth, M. The supramolecular organization of a peptide-based nanocarrier at high molecular detail. *J. Am. Chem. Soc.,* **2015,** *137*, 7775-7784.
70. Zhou, P.; Deng, L.; Wang, Y.; Lu, J. R.; Xu, H. Interplay between intrinsic conformational propensities and intermolecular interactions in the self-assembly of short surfactant-like peptides composed of leucine/isoleucine. *Langmuir,* **2016,** *32*, 4662-4672.
71. Iscen, A.; Schatz, G. C. Hofmeister Effects on Peptide Amphiphile Nanofiber Self-Assembly. *J. Phys. Chem. B,* **2019,** *123*, 7006-7013.

72. Dana, A.; Tekinay, A. B.; Tekin, E. D. A comparison of peptide amphiphile nanofiber macromolecular assembly strategies. *Eur. Phys. J. E,* **2019,** *42*, 63.
73. Lai, C.-T.; Rosi, N. L.; Schatz, G. C. All-Atom Molecular Dynamics Simulations of Peptide Amphiphile Assemblies That Spontaneously Form Twisted and Helical Ribbon Structures. *J. Phys. Chem. Lett.,* **2017,** *8*, 2170-2174.
74. Lee, O.-S.; Stupp, S. I.; Schatz, G. C. Atomistic Molecular Dynamics Simulations of Peptide Amphiphile Self-Assembly into Cylindrical Nanofibers. *J. Am. Chem. Soc.,* **2011,** *133*, 3677-3683.
75. Mehralitabar, H.; Taghdir, M.; Naderi-Manesh, H. A combination of bioactive and nonbioactive alkyl-peptides form a more stable nanofiber structure for differentiating neural stem cells: a molecular dynamics simulation survey. *J. Biomol. Struct. Dyn.,* **2019**, 1-11.
76. Tekin, E. D. Molecular dynamics simulations of self-assembled peptide amphiphile based cylindrical nanofibers. *RSC Advances,* **2015,** *5*, 66582-66590.
77. Deshmukh, S. A.; Solomon, L. A.; Kamath, G.; Fry, H. C.; Sankaranarayanan, S. K. Water ordering controls the dynamic equilibrium of micelle–fibre formation in self-assembly of peptide amphiphiles. *Nat. Commun.,* **2016,** *7*, 12367.
78. Lee, O.-S.; Liu, Y.; Schatz, G. C. Molecular dynamics simulation of β-sheet formation in self-assembled peptide amphiphile fibers. *J. Nanopart. Res.,* **2012,** *14*, 1-7.
79. Yu, T.; Schatz, G. C. Free Energy Profile and Mechanism of Self-Assembly of Peptide Amphiphiles Based on a Collective Assembly Coordinate. *J. Phys. Chem. B,* **2013,** *117*, 9004-9013.
80. Yu, T.; Lee, O. S.; Schatz, G. C. Steered Molecular Dynamics Studies of the Potential of Mean Force for Peptide Amphiphile Self-Assembly into Cylindrical Nanofibers. *J. Phys. Chem. A,* **2013,** *117*, 7453-7460.
81. Marrink, S. J.; Risselada, H. J.; Yefimov, S.; Tieleman, D. P.; de Vries, A. H. The MARTINI Force Field: Coarse Grained Model for Biomolecular Simulations. *J. Phys. Chem. B,* **2007,** *111*, 7812-7824.
82. Monticelli, L.; Kandasamy, S. K.; Periole, X.; Larson, R. G.; Tieleman, D. P.; Marrink, S.-J. The MARTINI Coarse-Grained Force Field: Extension to Proteins. *J. Chem. Theory Comput.,* **2008,** *4*, 819-834.
83. de Jong, D. H.; Singh, G.; Bennett, W. F. D.; Arnarez, C.; Wassenaar, T. A.; Schäfer, L. V.; Periole, X.; Tieleman, D. P.; Marrink, S. J. Improved Parameters for the Martini Coarse-Grained Protein Force Field. *J. Chem. Theory Comput.,* **2013,** *9*, 687-697.
84. Scott, G. G.; McKnight, P. J.; Tuttle, T.; Ulijn, R. V. Tripeptide Emulsifiers. *Adv. Mater,* **2016,** *28*, 1381-1386.
85. Sasselli, I. R.; Moreira, I. P.; Ulijn, R. V.; Tuttle, T. Molecular dynamics simulations reveal disruptive self-assembly in dynamic peptide libraries. *Org. Biomol. Chem.,* **2017,** *15*, 6541-6547.
86. Guo, C.; Luo, Y.; Zhou, R.; Wei, G. Probing the Self-Assembly Mechanism of Diphenylalanine-Based Peptide Nanovesicles and Nanotubes. *ACS Nano,* **2012,** *6*, 3907-3918.
87. Moreira, I. P.; Piskorz, T. K.; van Esch, J. H.; Tuttle, T.; Ulijn, R. V. Biocatalytic self-assembly of tripeptide gels and emulsions. *Langmuir,* **2017,** *33*, 4986-4995.
88. Frederix, P. W. J. M.; Ulijn, R. V.; Hunt, N. T.; Tuttle, T. Virtual Screening for Dipeptide Aggregation: Toward Predictive Tools for Peptide Self-Assembly. *J. Phys. Chem. Lett.,* **2011,** *2*, 2380-2384.
89. Frederix, P. W. J. M.; Scott, G. G.; Abul-Haija, Y. M.; Kalafatovic, D.; Pappas, C. G.; Javid, N.; Hunt, N. T.; Ulijn, R. V.; Tuttle, T. Exploring the Sequence Space for (Tri-)peptide Self-assembly to Design and Discover New Hydrogels. *Nat. Chem.,* **2015,** *7*, 30-37.
90. Guo, C.; Arnon, Z. A.; Qi, R.; Zhang, Q.; Adler-Abramovich, L.; Gazit, E.; Wei, G. Expanding the Nanoarchitectural Diversity Through Aromatic Di-and Tri-Peptide Coassembly: Nanostructures and Molecular Mechanisms. *ACS Nano,* **2016,** *10*, 8316-8324.
91. Lee, O.-S.; Cho, V.; Schatz, G. C. Modeling the Self-Assembly of Peptide Amphiphiles into Fibers Using Coarse-Grained Molecular Dynamics. *Nano Lett.,* **2012,** *12*, 4907-4913.
92. Yu, T.; Schatz, G. C. Free-Energy Landscape for Peptide Amphiphile Self-Assembly: Stepwise versus Continuous Assembly Mechanisms. *J. Phys. Chem. B,* **2013,** *117*, 14059-14064.
93. Velichko, Y. S.; Stupp, S. I.; Olvera de la Cruz, M. Molecular simulation study of peptide amphiphile self-assembly. *J. Phys. Chem. B,* **2008,** *112*, 2326-2334.
94. Pappas, C. G.; Sasselli, I. R.; Ulijn, R. V. Biocatalytic pathway selection in transient tripeptide nanostructures. *Angew. Chem.,* **2015,** *127*, 8237-8241.
95. Marchesan, S.; Easton, C. D.; Styan, K.; Waddington, L.-.; Kushkaki, K.; Goodall, L.; McLean, K.; Forsythe, J. S.; Hartley, P. G. Chirality effects at each amino acid position on tripeptide self-assembly into hydrogel biomaterials. *Nanoscale,* **2014,** *6*, 5172-5180.

96. Marchesan, S.; Waddington, L.; Easton, C. D.; Winkler, D. A.; Goodall, L.; Forsythe, J.; Hartley, P. G. Unzipping the role of chirality in nanoscale self-assembly of tripeptide hydrogels. *Nanoscale,* **2012,** *4*, 6752-6760.
97. Hanwell, M. D.; Curtis, D. E.; Lonie, D. C.; Vandermeersch, T.; Zurek, E.; Hutchison, G. R. Avogadro: an advanced semantic chemical editor, visualization, and analysis platform. *J. Cheminform.,* **2012,** *4*, 17.
98. *martinize.py*, 2.0; <http://cgmartini.nl/images/tools/martinize/martinize-2.6/martinize.py>.
99. Abraham, M. J.; Murtola, T.; Schulz, R.; Páll, S.; Smith, J. C.; Hess, B.; Lindahl, E. GROMACS: High performance molecular simulations through multi-level parallelism from laptops to supercomputers. *SoftwareX,* **2015,** *1*, 19-25.
100. Berendsen, H. J. C.; van der Spoel, D.; van Drunen, R. GROMACS: A message-passing parallel molecular dynamics implementation. *Comput. Phys. Commun.,* **1995,** *91*, 43-56.
101. Humphrey, W.; Dalke, A.; Schulten, K. VMD: Visual molecular dynamics. *J. Mol. Graphics,* **1996,** *14*, 33-38.
102. Mayans, E.; Ballano, G.; Casanovas, J.; Díaz, A.; Pérez-Madrigal, M. M.; Estrany, F.; Puiggalí, J.; Cativiela, C.; Alemán, C. Self-Assembly of Tetraphenylalanine Peptides. *Chem.-Eur. J.,* **2015,** *21*, 16895-16905.
103. Matson, J. B.; Newcomb, C. J.; Bitton, R.; Stupp, S. I. Nanostructure-templated control of drug release from peptide amphiphile nanofiber gels. *Soft Matter,* **2012,** *8*, 3586-3595.